



Selective deposition of chemically-bonded gold electrodes onto PDMS microchannel side walls



Andrea L. Kadilak^a, Ying Liu^a, Sujan Shrestha^a, Joshua R. Bernard^a, William E. Mustain^a, Leslie M. Shor^{a,b,*}

^a Department of Chemical & Biomolecular Engineering, University of Connecticut, Storrs, CT, USA

^b Center for Environmental Sciences & Engineering, University of Connecticut, Storrs, CT, USA

ARTICLE INFO

Article history:

Received 11 March 2014

Received in revised form 28 May 2014

Accepted 3 June 2014

Available online 14 June 2014

Keywords:

Electrode

Gold

MEMS

Microfluidic

Microfabrication

ABSTRACT

Many applications of microfluidic devices require the incorporation of electrodes. In this paper, we describe the simulation, fabrication, and performance of gold electrodes selectively deposited on the side walls of a microchannel. Electrode microfabrication methods typically pattern metal electrodes onto a flat substrate. However, when anode and cathode are both positioned on the bottom of a microfluidic channel, the electric field is not uniform with channel depth. Finite element modeling was used to characterize field distortion for conventional electrode placement vs. side wall positioning for a range of microchannel geometries. These models showed that electrodes located on microchannel side walls created an electric field that was uniform with depth at all points within the channel, while electrodes deposited on the bottom substrate resulted in a 10–40% decrease in potential vertically along the microchannel side wall. This paper also demonstrates a new fabrication method to chemically bonded gold electrodes along opposing vertical side walls in a closed PDMS microchannel. Deposition of gold on the PDMS microchannel side walls was confirmed by SEM/EDX imaging and electrochemical analysis. Fabricated electrodes were electrochemically stable and resistant to shear.

© 2014 Elsevier B.V. All rights reserved.

1. Introduction

Electrodes add functionality in many microfluidic applications. Microfluidic devices may incorporate electrodes for chemical or biological sensing [1–7], for particle separations [7–9], to drive electroosmotic flow [10,11], or for power generation in microfluidic fuel cells [12–17]. In a microfluidic system, electrodes must be fabricated to interface properly with other device features and functionalities. For example, electrode placement should not interfere with optical assays. Additionally, electrodes should be durably attached and materials often must be compatible with living cells

and other reactive biological and chemical agents that pass through the device.

Gold is the most common material used in microfluidic electrodes due to its high electrical conductivity, chemical inertness, and good biocompatibility. Well-developed photolithography-based methods exist to pattern gold or other conductive materials onto flat surfaces, which can be used as the bottom substrate upon which microfluidic channels are bonded. The most commonly used techniques combine photolithography with either etching or lift off [18,19]. In etching, the conductive material is deposited first, and then photoresist is applied on top and patterned, acting as a protective mask. Lift-off methods pattern the photoresist first and then use the photoresist as a stencil to pattern the metal. Additionally, surface modification via UV-initiated graft-polymerization and amination has been demonstrated to photopattern and chemically bond gold onto a flat polydimethylsiloxane (PDMS) substrate [20] and a flat polystyrene (PS) substrate [7].

In the preceding examples, the electrodes are patterned on an open, flat surface. To incorporate such electrodes within a microfluidic device, the fluidic layer must be aligned with and bonded to the electrode-patterned substrate, which may be difficult to do with

Abbreviations: PDMS, polydimethylsiloxane; CB, carbon black; AA, acrylic acid; PAA, poly(acrylic acid); BP, benzophenone; ATR-FTIR, attenuated total reflectance Fourier transform infrared; EDA, ethylenediamine; EDC, N-(3-dimethylaminopropyl)-N'-ethylcarbodiimide hydrochloride; EDX, energy-dispersive X-ray spectroscopy; CV, cyclic voltammogram.

* Corresponding author at: Department of Chemical & Biomolecular Engineering, University of Connecticut, 191 Auditorium Road, Unit 3222, Storrs, CT 06269-3222, USA. Tel.: +1 (860) 486 3136.

E-mail address: leslieshor@gmail.com (L.M. Shor).

the required precision. Another important drawback to electrodes patterned on the bottom surface of the channel is that the resulting electric field is not uniform with depth (Fig. 1A). Thus, chemicals or cells experience different potentials at different depths in the microchannel, which can adversely affect performance in microfluidic applications such as electrophoretic separations.

In addition to photolithography combined with etching or lift-off, several other techniques have been used to incorporate electrodes in microfluidic devices. For example, silver wires have been introduced through guide channels, resulting in electrode wires laying along the bottom corners of the microfluidic channels [21]. One possible difficulty with this approach is poor precision in the electrode placement, which can lead to misalignment with side walls, reduction in efficacy, and short-circuiting. Even if ideally positioned along the bottom corners of the channel, wire electrodes result in similarly distorted electric fields as pad-type electrodes (Fig. 1B).

In contrast to the substrate-patterned and wire electrode examples discussed above, an ideal electrode configuration would result in a uniform potential gradient along the width and depth of the microfluidic channel. This ideal configuration can be achieved with electrodes fabricated along only the side walls of a microfluidic channel. Fig. 1C illustrates the ideal electric field generated when electrodes are located along the vertical side walls of the microchannel, in contrast with the distorted electric field resulting from traditional pad or wire electrodes shown in Fig. 1A and B. A more extensive theoretical basis and discussion on the advantages of side wall electrodes is provided in Section 3.

Other investigators have created electrodes along the inner surfaces of microfluidic channels. Mustin and Stoeber created electrodes in a microfluidic channel by casting PDMS devices with carbon black-rich patches [22]. In their report, electrodes were positioned within, not along the outer edge of, flow channels. Their method permits users without access to specialized microfabrication tools to implement a variety of 3D electrode geometries and to avoid alignment and bonding problems common for substrate-patterned pad electrodes. However, the conductivity of carbon black in PDMS is much lower than that of gold, especially at the low carbon black loadings needed for that method. Poor biocompatibility of carbon black may also be problematic for certain applications. In several reports, Arriaga and coworkers spray-coated a conductive “ink” along the side walls of millimeter-scale channels hot embossed into poly(methyl methacrylate) [14–17]. However, successful implementation of spray coating techniques into sealed microchannels may prove challenging. Further, realization of a working electrode requires additional microfabrication steps that may be difficult to implement inside a closed microfluidic channel. Finally, spray-coating may not be as resistant to shear as chemically-bonding gold uniformly on the interior side walls of a microdevice.

In this paper, we demonstrate a new method to create chemically bonded gold electrodes along vertical side walls of a PDMS microchannel (Fig. 1D). PDMS is one of the most commonly used materials for biological applications of microfluidic devices because it is optically transparent, biocompatible, and is permeable to oxygen and carbon dioxide. Surface-directed graft polymerization

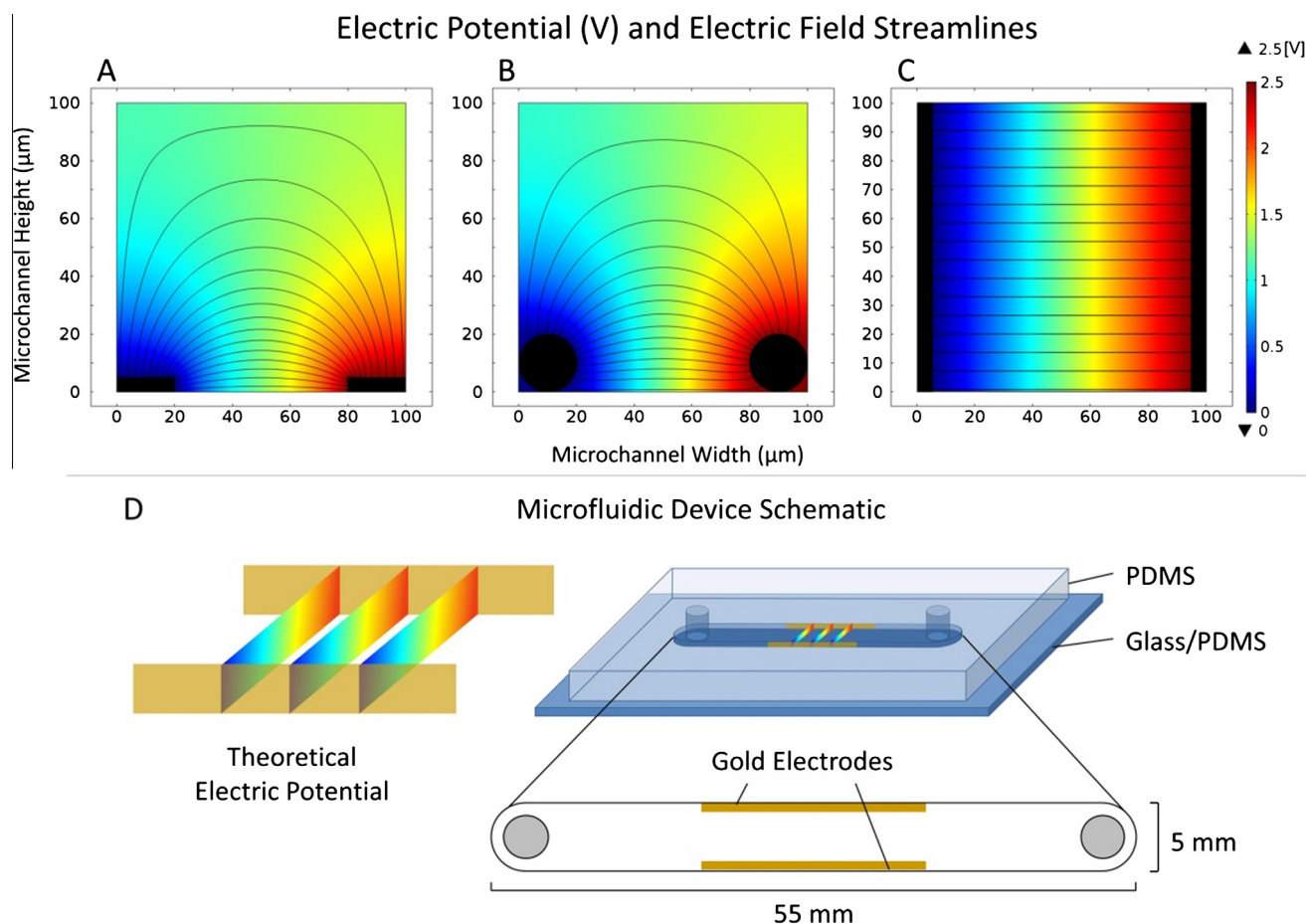


Fig. 1. Panels A–C illustrate the potential (V) and electric field lines modeled using COMSOL Multiphysics 4.3b for a $100 \times 100 \mu\text{m}$ cross-section of a microchannel where (A) represents electrode pads ($5 \times 20 \mu\text{m}$), (B) represents wire electrodes (radius = $10 \mu\text{m}$), and (C) represents an ideal, conformally-coated electrode on the side walls of the channel. Panel (D) is a schematic of the microfluidic device used in this paper (microchannel dimensions 5 mm wide \times 55 mm long \times 100 μm high).

and further surface chemistry modification to deposit gold on PDMS has been previously described by Hao et al. [20], who patterned gold on a flat PDMS substrate. We describe a method to fabricate and pattern gold electrodes inside a closed PDMS microchannel. In this fabrication procedure, photopatterning initiated the selective formation of the gold electrode layer along only the side walls of the closed microfluidic channel. The presence of gold on the microchannel side walls was verified using SEM/EDX. The gold-patterned side walls functioned as electrodes as demonstrated by cyclic voltammetry performed both before and after gold deposition, and before and after shear resistance testing. This method relies on photolithography equipment, materials, and techniques that are already in wide use in microfabrication labs, making it readily adaptable to various microfluidic applications.

2. Materials and methods

2.1. Chemicals

Sylgard 184 silicone elastomer kit (PDMS) was purchased from Dow Corning (Midland, MI). SU-8 2100 photoresist and SU-8 developer were obtained from Microchem (Newton, MA). Benzophenone (99%), acrylic acid (99%), ethylenediamine ($\geq 99.5\%$), and N-(3-dimethylaminopropyl)-N'-ethylcarbodiimide hydrochloride ($\geq 99.0\%$) were purchased from Sigma–Aldrich. Gold (III) chloride trihydrate, sodium sulfite, sodium thiosulfate ($\geq 98.0\%$), potassium thiocyanate, ascorbic acid (99%), and sodium borohydride ($\geq 98\%$) were purchased from Fisher Scientific. All chemicals were used as received. The electrical connects were conducting composites comprised of PDMS mixed with carbon black (CB) (Carbon black, Vulcan XC72-R, Cabot Corporation) and hexane ($\geq 95\%$, Sigma–Aldrich). Deionized (DI) water (resistivity $\geq 18.2 \text{ M}\Omega \text{ cm}$) was produced from a Direct-Q 3 UV Millipore ultrapure water system.

2.2. Preparation of microfluidic flow cell

A schematic for the microfluidic device described in this paper is presented in Fig. 1D. The dimensions of the channel were 5 mm wide by 55 mm long and the height measured $96 \pm 13 \mu\text{m}$ (Dektak surface profilometer Model 150, Veeco Instruments, Plainview NY). The channel contained two rows of posts measuring $200 \mu\text{m}$ in diameter. Microfluidic masters were created from SU-8 2100 (Microchem, Newton, MA) using photolithography as previously described [23]. Detailed fabrication parameters can be found in Table S-1. Mylar photomasks were purchased from Advanced Reproduction (Andover, MA) and silicon wafers from Nova Electronic Materials (test grade, Flower Mound, TX).

Replicate devices were cast from masters in PDMS using standard soft lithography methods [24]. Briefly, a 10:1 mixture of PDMS polymer base and curing agent was fully mixed, de-gassed, then poured over the masters and cured in place for 4 h at 60°C . Castings were peeled away from the master, access ports were punched with a biopsy punch, and each device was irreversibly bonded to either a glass microscope slide or a thin slab of PDMS by exposing both surfaces to oxygen plasma (Plasma Cleaner model PDC-32G, Harrick Plasma, Ithaca, NY) for 30 s or 45 s, respectively. Deionized water was immediately added to the microchannel to maintain the hydrophilicity of the PDMS [25].

2.3. Deposition of carbon black-PDMS electrical connects

To enable electrochemical characterization of the gold side wall electrodes, non-gold leads were needed to connect side wall

electrodes with an external power source. Electrical connects comprised of a conductive CB-PDMS composite were fabricated on the substrate prior to microfluidic flow cell assembly. First, 0.2 g PDMS base, 0.02 g curing agent, 0.1 g CB, and 1 ml hexane were combined in a sealed glass vial containing a microstir bar. Mixing was achieved by alternating 15 min of micromagnetic stirring with 15 min sonication. The CB-PDMS electrical connects were then patterned using a spray gun (Badger Air-Brush Co., Franklin Park, IL) to deposit the CB-PDMS over a masked glass substrate which was then cured for 4 h at 60°C . Before further treatment, the substrate was rinsed with isopropanol and dried with N_2 gas to remove impurities. The conductivity of this CB-PDMS layer averaged $40 \pm 2 \text{ S m}^{-1}$.

To facilitate bonding the microfluidic flow cell to the CB-PDMS connects, a thin PDMS coating was spray-coated over most of the conducting strips by masking and spraying as before. The extreme inner edges of the CB-PDMS electrodes were masked prior to depositing the PDMS coating to ensure electrical contact with gold side wall electrodes in the completed device. The PDMS coating was comprised of a uniform mixture of 0.1 g PDMS base, 0.01 g curing agent, and 0.5 ml hexane. The PDMS coating was partially cured at room temperature for approximately 3 h prior to final assembly of the microfluidic device.

2.4. Fabrication of gold side wall electrodes

The selective deposition of chemically-bonded gold electrodes on the side walls of the PDMS device required several steps. The UV-induced graft polymerization of acrylic acid (AA) to polyacrylic acid (PAA) in the presence of the photoinitiator, benzophenone (BP), absorbed in PDMS was originally developed by the Allbritton et al. [26,27] and Tabeling et al. [28,29] groups, who established process parameters required for successful polymerization within a PDMS microchannel. Hao et al. [20] developed a method to combine this chemistry with amination and growth steps to photopattern a gold film on a flat PDMS substrate. The procedure described here combined and adapted these previous methods to a flowing system inside a PDMS microfluidic channel.

A custom photomask was used to selectively initiate graft polymerization of AA to PAA in the presence of BP, the photoinitiator. Prior to photopatterning, a solution of BP in acetone was flowed through the microchannel; the acetone solvent causes slight swelling in the PDMS device, allowing the BP to move into the cross-linked polymer network. Any remaining acetone was evaporated and then the channel was loaded with a de-aerated AA solution. At this point, the AA in the microchannel was only in contact with the BP photoinitiator at the interior PDMS channel surface. Photopatterning was achieved by aligning transparent regions of the photomask with the side walls of the filled PDMS microchannel. After polymerization, the PAA was surface-functionalized with an amine group to allow for the attachment of a gold seed layer. The final gold electrodes were then grown by electroless deposition. A schematic of the overall protocol is presented in Fig. 2. Table S-2 lists the chemicals, concentrations, flow rates, and additional process parameters for each step including grafting of PAA, preparation of PAA graft for gold deposition, and formation of gold electrodes. Each step of the process is described in detail in Supplemental Information.

2.5. Confirming PDMS surface modification with ATR-FTIR

Polymerization of PAA along the PDMS side walls and surface chemistry modifications after the amination step were confirmed using attenuated total reflectance Fourier transform infrared (ATR-FTIR) spectroscopy (iS10 spectrometer, Thermo Scientific).

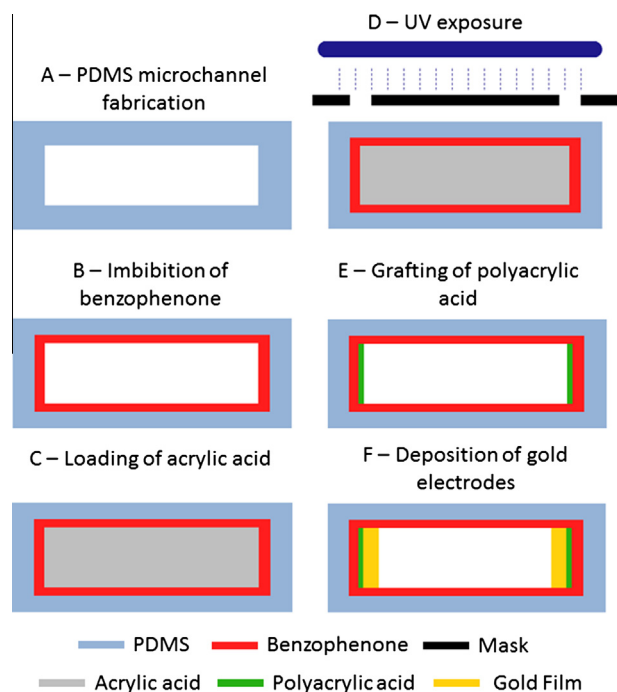


Fig. 2. Schematic of fabrication of gold electrodes on the side walls of a PDMS microchannel. Each panel depicts a cross-section of the microfluidic channel, where into the page is in the direction of flow through the channel. (A) Initial cross-section of a PDMS microchannel (light blue). (B) PDMS microchannel imbibed with benzophenone (red). (C) The microchannel filled with acrylic acid (gray). (D) Region-selective UV exposure (blue) along the side walls only using a photomask (black). (E) Polyacrylic acid (green) grafted on the side walls. (F) Formation of gold film (yellow) on the side walls after amination, nucleation, and growth of the gold film. (For interpretation of the references to colour in this figure legend, the reader is referred to the web version of this article.)

2.6. Confirming gold deposition with SEM/EDX

The Au layer formed along the PDMS microchannel side walls could be observed directly and was further characterized using a JEOL JSM-6330F scanning electron microscope (SEM) equipped with Thermo Noran System Six energy-dispersive X-ray spectroscopy (EDX) system. A thin transverse section of the coated microchannel was sectioned using a razor blade, placed on a glass microscope coverslip, sputtered with carbon using an Edwards 306A vacuum evaporator, and then imaged.

2.7. Electrochemical characterization of the PDMS microdevice

All electrochemical experiments were carried out in N_2 -saturated 0.1 M $HClO_4$ at room temperature using an Autolab PGSTAT302N potentiostat. The PDMS microdevice was connected to the potentiostat by two electrical clips connected to the CB-PDMS conducting strips. At least 5 cyclic voltammograms (CVs) were run between -2.0 and 2.0 V at 100 mV/s to condition the Au electrodes prior to data collection.

3. Theoretical basis and simulation of electrode performance

Steady-state electric fields within a microfluidic channel were simulated in COMSOL Multiphysics 4.3b using the Electrostatics physics package. Electrodes were modeled along the channel substrate in a configuration typical for microfabricated pad

electrodes (20×5 μm , Fig. 1A), wall-aligned wire electrodes (10 μm radius, Fig. 1B), or as the ideal side wall configuration proposed here (5×100 μm , Fig. 1C). For all simulations, the 2-D cross-section of the flow channel was modeled as a rectangle with a height of 100 μm . Simulations were conducted with four aspect ratios of height to width: 1:1, 1:2, 1:5, and 1:10; these ratios corresponded to microchannel widths of 100 , 200 , 500 , and 1000 μm in the simulation. The device was assumed to be electrically insulated, and the microchannel was filled with water with an isotropic relative permittivity of 80. The potential difference between the two electrodes was 2.5 V in all simulations. For each aspect ratio and electrode configuration, the potential was evaluated as a function of height within the channel at various distances from the vertical side wall of the device: at the wall and at distances 10%, 20%, and 50% of the total channel width away from the wall.

Finite element simulations for the four aspect ratios clearly illustrated the advantages of electrodes located along the vertical side walls compared with electrodes located on the bottom surface. For microchannels in which the electrodes were located on the side walls, the potential was constant along the vertical axis (Fig. 3). For ideal side wall electrodes, the magnitude of the potential at different positions across the channel differed slightly for different aspect ratios since the electric field in water is not perfectly linear. However, for microchannels with 5×20 μm pad and 10 μm radius wire electrodes, there were large variations in the potential along the vertical axis at nearly all distances from the wall. A sizeable reduction in potential along the side wall edge opposite a substrate-bonded electrode was observed for these electrode configurations. As shown in Fig. 3, the variation in the electric field was greatest in microchannels with smaller aspect ratios (i.e., 1:1 and 1:2), and was greatest near the side walls. For example, in channels with a 1:1 aspect ratio, there was approximately a 45% reduction in potential along a vertical transect located 20 μm (20% transect) from the side of the 100 μm channel. Similarly, in channels with a 1:2 aspect ratio, there was approximately a 30% reduction in potential along a vertical transect located 20 μm (10% transect) from the side wall of the 200 μm channel. As the aspect ratio of the channel increased, the middle of the channel exhibited behavior closer to that of the ideal side wall deposited electrodes.

However, even in higher aspect ratio channels (i.e., 1:5 and 1:10), vertical inhomogeneity of the electric field could be observed 50 μm or more from the side wall for pad-type electrodes; this number is significant when compared to the size of microscopic species that may be observed, separated, or otherwise subjected to the electric field. Thus, in a real device with pad or wire electrodes, the potential experienced by cells, ions or any other species, particularly those located near the side walls, could differ substantially with height within the microchannel. In contrast, electrodes positioned along the vertical side walls of a microfluidic channel result in a vertically consistent electric field, regardless of microchannel dimensions or position along the microchannel width. Vertical homogeneity in the electric field will allow for microfluidic devices with enhanced separations efficiency, more sensitive electrochemical sensing capabilities, and more uniform electro-osmotic flow.

One possible method for experimentally validating the vertical uniformity of the electrical field is by imaging the response of charged fluorescent tracers while applying a current to the electrodes [30]. Using a confocal microscope, one could image the distribution of the tracers in the channel at different points along the vertical axis for the two different electrode configurations (side wall vs. pad electrodes).

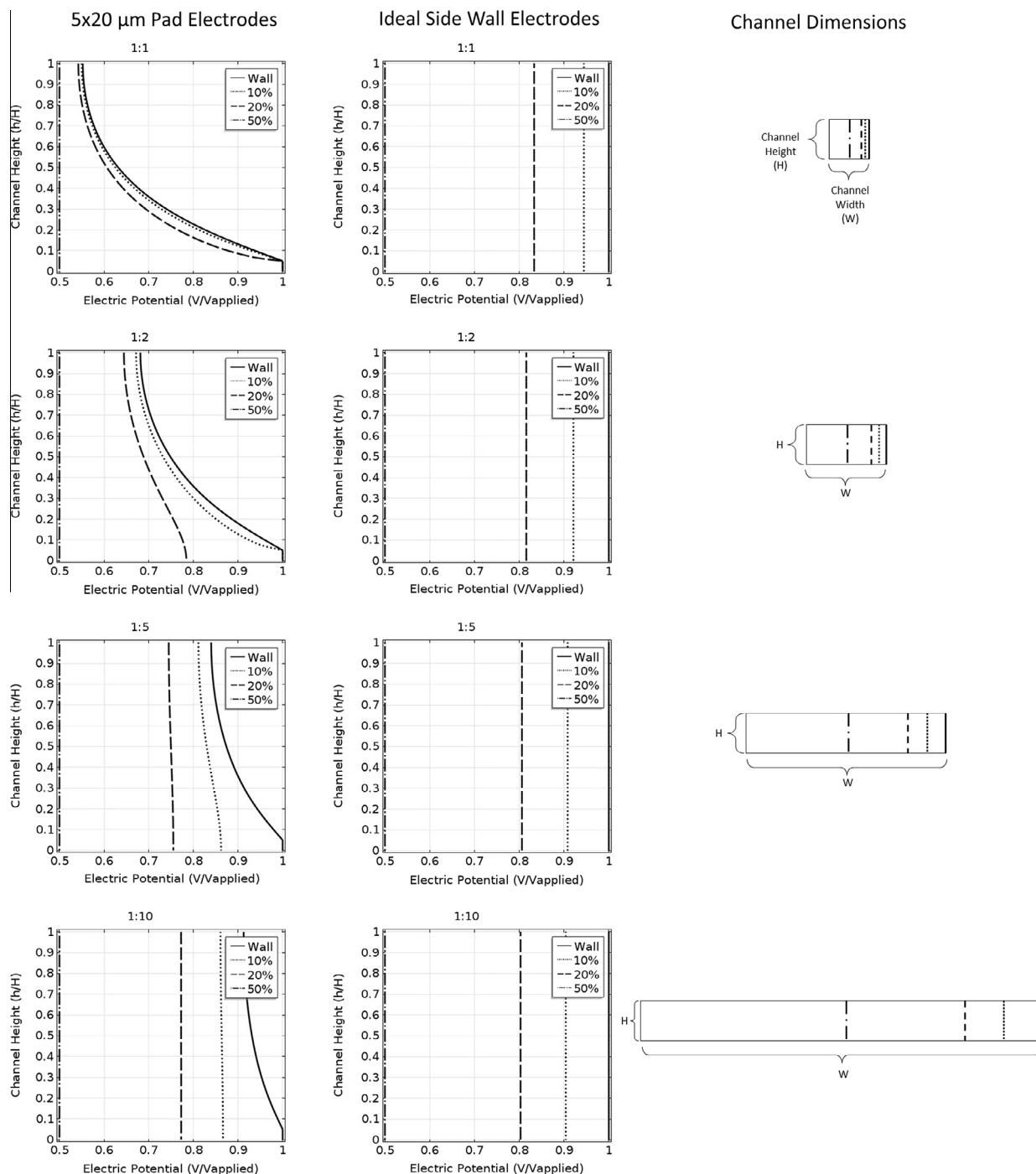


Fig. 3. Electric potential along vertical transects of microchannels with aspect ratios ($h:w$) of 1:1, 1:2, 1:5, and 1:10 modeled in COMSOL Multiphysics 4.3b. Transects are located at the right side wall and distances 10%, 20%, and 50% of the total channel width from the wall, as illustrated on the right. For example, for a 100 μm wide channel, transects would be 10, 20, and 50 μm from the wall. These plots illustrate the disturbance in the potential in the vertical direction for pad electrodes deposited on the substrate on the bottom surface of the microchannel compared to the stability of the electrodes deposited on the side walls of the channel.

4. Results and discussion

4.1. Confirmation of PDMS surface functionalization and gold deposition

ATR-FTIR spectra were collected on disassembled PDMS microchannels at interim steps of the side wall electrode fabrication and were compared with untreated samples. Results are shown in Fig. S-2. The polymerization of AA to PAA after exposure to UV was shown by the broadening of the peak near 3000 cm^{-1} , which is indicative of carboxyl ($-\text{COOH}$) stretching. The sharp peak at

1700 cm^{-1} was consistent with carbonyl ($-\text{C}=\text{O}$) stretching. Both features were absent from the bare PDMS and UV-exposed untreated PDMS, confirming the formation of PAA in the treated sample. Peaks due to carbonyl stretching in an amide group were evident at 1550 cm^{-1} after amination. In addition, the broad peak at 3200 cm^{-1} was assigned to N-H stretching. ATR-FTIR showed that the described procedure successfully functionalized the PDMS surface with amine groups.

The formation of the Au seed layer was visually apparent as dark lines along the sides of the microchannel (Fig. S-3). Minimal deposition was observed on the substrate or the top of the

microchannel. The localization along the side walls showed site-selective deposition of Au. Selective deposition of Au along the microchannel side wall was confirmed by SEM images and EDX of microchannel cross-sections (Figs. 4 and S-3). A slight curvature in the PDMS side wall could be observed in the SEM image, and was likely an artifact from the cross-sectioning procedure or possibly caused by a slight vertical slant in the master mold for the microfluidic device. In the SEM image, the Au film could be clearly seen as a bright lining along the side wall of the microchannel. The presence of Au in this location was verified using EDX elemental mapping. As can be seen in Fig. 4, silicon (Si) that makes up a portion of the PDMS polymer backbone was distributed throughout the entire microfluidic channel, as expected. Furthermore, the elemental mapping verified that the bright lining in the SEM image was not merely an edge effect, but was indeed an Au film, selectively deposited only along the vertical side wall (Fig. 4). The measured thickness of the film was approximately 4 μm and consistent over the height of the channel in multiple cross-sections sampled from multiple devices. The electric field was modeled considering various possible defects in the side wall electrodes, including

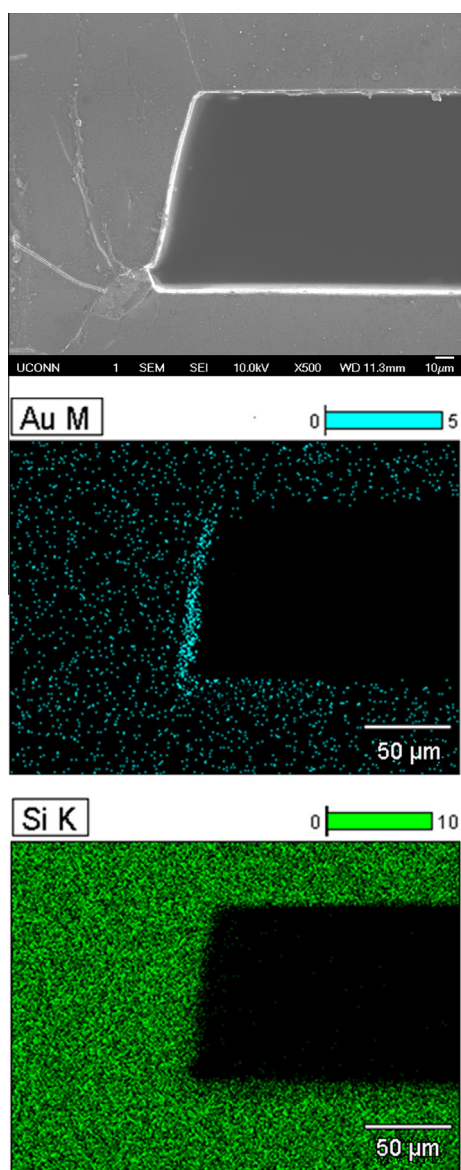


Fig. 4. SEM image and EDX mapping showing a cross-section of a PDMS microchannel with the gold film deposited selectively at the side walls.

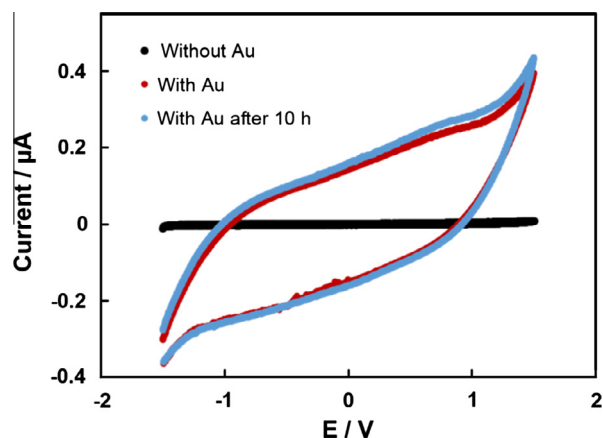


Fig. 5. Cyclic voltammograms of the PDMS microdevice with CB-PDMS electrical connects but without gold side wall electrodes (black), with gold side wall electrodes (red), and with gold side wall electrodes after 10 h shear test (blue) in flowing 0.1 M N_2 -saturated HClO_4 . The scan rate used during cyclic voltammograms was 20 mV s^{-1} and the flow rate used for the shear test was $200 \mu\text{l/min}$. (For interpretation of the references to colour in this figure legend, the reader is referred to the web version of this article.)

surface roughness, slanted electrodes, and electrodes with over-patterning on the channel top and bottom; even with these defects, the side wall electrodes demonstrated a uniform electric field compared to pad and wire electrodes (Fig. S-4).

4.2. Electrochemical characterization of the PDMS microdevice

The electrochemical responses of the PDMS microdevices with and without deposited Au on the side walls were measured under flow of 0.1 M N_2 -saturated HClO_4 . Fig. 5 shows cyclic voltammograms of freshly-prepared PDMS microdevices without (black) and with gold electrodes on the inner side walls (red). For electrodes without deposited Au, only a very small capacitive current was observed with a small amount of oxygen evolution starting around 1.5 V. This very small current was due to the presence of exposed carbon from the CB-PDMS connects. For microdevices with Au side wall electrodes, there were two obvious changes in the voltammogram. First, the capacitive current was increased, suggesting that the deposited Au had a high surface area, which was observed with the SEM images in Fig. 4. The second significant change in the voltammogram was a decrease in the onset potential for oxygen evolution to approximately 1.1 V, confirming the activity of the deposited Au. One interesting aspect of the recorded CVs was the lack of characteristic oxidation peaks that are commonly observed for polycrystalline Au, which shows that the deposited Au was active despite being poorly crystallized.

To determine the physical stability of the deposited Au layer and its resistance to shear, DI water was flowed through the channel at $200 \mu\text{l min}^{-1}$ for 10 h. The cyclic voltammogram of the post-sheared device is shown as the blue curve in Fig. 5, which is nearly the same as the freshly-prepared device (red). This showed that the chemically-bonded Au side wall electrodes were stable in the presence of shear.

5. Conclusion

In this report, a method is described to fabricate chemically-bonded Au electrodes along only the side walls of a PMDS microfluidic device. CB-PDMS electrical contacts were used to connect the electrodes to the external circuit. We showed that the electrodes were electrochemically active and resistant to shear. Computer simulations proved that side wall electrodes prevent

the vertical inhomogeneity of the electric field that occurs with substrate-patterned electrodes. The homogeneous electric field enabled by the reported sidewalls can increase the sensitivity of microfluidic separations and enable more electroosmotic separations. These electrodes may also be beneficial for microfluidic fuel cells and electrosynthesis.

Certain limitations to this method exist, including the large size of the microchannel used. Such a wide channel was used to facilitate manual alignment of the photomask in the PAA photopolymerizing step, but is not representative of the scale used in many microfluidic applications. Additionally, the lack of precision in the spray coating method used to deposit the CB electrical connects led to occasional issues in microchannel bonding and alignment. Future work will focus on refining the procedure for improved precision in smaller microfluidic channels; implementing photo-patterned Au electrical connects for improved performance, biocompatibility, and streamlined assembly; and application-specific evaluation.

Conflict of interest

There is no conflict of interest.

Acknowledgements

The authors gratefully acknowledge financial support from NSF EFRI award 1137249 and fellowship support to Andrea Kadilak through NSF GK-12 award 0947869.

Appendix A. Supplementary material

Supplementary data associated with this article can be found, in the online version, at <http://dx.doi.org/10.1016/j.jelechem.2014.06.006>.

References

- [1] F.A. Bertolino, I.E. De Vito, G.A. Messina, H. Fernández, J. Raba, J. Electroanal. Chem. 651 (2011) 204–210.
- [2] E. Bitziou, M.E. Snowden, M.B. Joseph, S.J. Leigh, J.A. Covington, J.V. Macpherson, P.R. Unwin, J. Electroanal. Chem. 692 (2013) 72–79.
- [3] X. Zhang, C. Chen, J. Li, L. Zhang, E. Wang, Anal. Chem. 85 (2013) 5335–5339.
- [4] J. Parisi, L. Su, Y. Lei, Lab Chip 13 (2013) 1501–1508.
- [5] Y.J. Kim, J.E. Jones, H. Li, H. Yampara-Iquise, G. Zheng, C.A. Carson, M. Cooperstock, M. Sherman, Q. Yu, J. Electroanal. Chem. 702 (2013) 72–78.
- [6] A. Sahin, K. Dooley, D.M. Crokek, A.C. West, S. Banta, Sensors Actuat. B: Chem. 158 (2011) 353–360.
- [7] X. Hu, Q. He, H. Lu, H. Chen, J. Electroanal. Chem. 638 (2010) 21–27.
- [8] N. Lewpiriyawong, K. Kandaswamy, C. Yang, V. Ivanov, R. Stocker, Anal. Chem. 83 (2011) 9579–9585.
- [9] S.H. Ling, Y.C. Lam, K.S. Chian, Anal. Chem. 84 (2012) 6463–6470.
- [10] J.S. Mellors, W.A. Black, A.G. Chambers, J.A. Starkey, N.A. Lacher, J.M. Ramsey, Anal. Chem. 85 (2013) 4100–4106.
- [11] J. Wu, K. Xu, J.P. Landers, S.G. Weber, Anal. Chem. 85 (2013) 3095–3103.
- [12] C.M. Moore, S.D. Minteer, R.S. Martin, Lab Chip 5 (2005) 218–225.
- [13] M.J. Gonzalez-Guerrero, J.P. Esquivel, D. Sanchez-Molas, P. Godignon, F.X. Munoz, F.J. del Campo, F. Giroud, S.D. Minteer, N. Sabate, Lab Chip 13 (2013) 2972–2979.
- [14] R. Galindo, A. Dector, L.G. Arriaga, S. Gutiérrez, P. Herrasti, J. Electroanal. Chem. 671 (2012) 38–43.
- [15] D. Morales-Acosta, H. Rodríguez, L.A. Godínez, L.G. Arriaga, J. Power Sources 195 (2010) 1862–1865.
- [16] F.M. Cuevas-Muniz, M. Guerra-Balcazar, J.P. Esquivel, N. Sabate, L.G. Arriaga, J. Ledesma-García, J. Power Sources 216 (2012) 297–303.
- [17] M. Guerra-Balcázar, D. Morales-Acosta, F. Castaneda, J. Ledesma-García, L.G. Arriaga, Electrochem. Commun. 12 (2010) 864–867.
- [18] L. Abad, F. Javier Del Campo, F.X. Munoz, L.J. Fernandez, D. Calavia, G. Colom, J.P. Salvador, M.P. Marco, V. Escamilla-Gomez, B. Esteban-Fernandez de Avila, S. Campuzano, M. Pedrero, J.M. Pingarron, N. Godino, R. Gorkin 3rd, J. Ducree, Electrophoresis 33 (2012).
- [19] P.J. Castle, P.W. Bohn, Anal. Chem. 77 (2005).
- [20] Z. Hao, H. Chen, D. Ma, Anal. Chem. 81 (2009) 8649–8653.
- [21] G.H. Kwon, Y.Y. Choi, J.Y. Park, D.H. Woo, K.B. Lee, J.H. Kim, S.H. Lee, Lab Chip 10 (2010) 1604–1610.
- [22] B. Mustin, B. Stoeber, Lab Chip 12 (2012) 4702–4708.
- [23] J. Deng, A. Dhummakupt, P.C. Samson, J.P. Wikswo, L.M. Shor, Anal. Chem. 85 (2013) 5411–5419.
- [24] G. Whitesides, E. Ostuni, S. Takayama, X. Jiang, D. Ingber, Annu. Rev. Biomed. Eng. 3 (2001) 335–373.
- [25] R. Mukhopadhyay, Anal. Chem. 79 (2007) 3248–3253.
- [26] S.W. Hu, X.Q. Ren, M. Bachman, C.E. Sims, G.P. Li, N.L. Allbritton, Anal. Chem. 76 (2004) 1865–1870.
- [27] Y.L. Wang, H.H. Lai, M. Bachman, C.E. Sims, G.P. Li, N.L. Allbritton, Anal. Chem. 77 (2005) 7539–7546.
- [28] M.H. Schneider, Y. Tran, P. Tabeling, Langmuir 27 (2011) 1232–1240.
- [29] M.H. Schneider, H. Willaime, Y. Tran, F. Rezzui, P. Tabeling, Anal. Chem. 82 (2010) 8848–8855.
- [30] U. Tallarek, E. Rapp, H. Sann, U. Reichl, A. Seidel-Morgenstern, Langmuir 19 (2003) 4527–4531.